Nuclear Instruments and Methods in Physics Research B 498 (2021) 27–33

Contents lists available at ScienceDirect

Nuclear Inst. and Methods in Physics Research, B

journal homepage: www.elsevier.com/locate/nimb

Effects of order and disorder on the defect evolution of NiFe binary alloys from atomistic simulations

Guojia Ge [a], Feida Chen [a,b], Xiaobin Tang [a,b,*], Changyuan Li [a], Jing Gao [a], Songyuan Li [a], Zhenlong Geng [a]

[a] Department of Nuclear Science & Technology, Nanjing University of Aeronautics and Astronautics, Nanjing 211106, PR China
[b] Key Laboratory of Nuclear Technology Application and Radiation Protection in Astronautics, Ministry of Industry and Information Technology, Nanjing, PR China

ARTICLE INFO

Keywords:
Order and disorder
Defect evolution
Molecular dynamics simulation
Interstitial diffusion
Dislocation-enhanced cascade

ABSTRACT

The effects of the ordered and disordered arrangements of elements on radiation-induced defects production and evolution in NiFe alloys were investigated through atomistic simulations. Results present a sluggish evolution of the overall microstructure in ordered $L1_0$ NiFe. Although the disordered phase has fewer Frankel pair accumulation in cascade simulation attributed to the low thermal conductivity reduced by the intrinsic chemical disorder, the difference is negligible when PKA energy increases because of the direct formation of clusters. Interstitial diffusion is restricted in the ordered phase, where Ni and Fe layers are alternately arranged. This condition delays interstitials accumulation and leads to the formation of more Shockley partial loops rather than Frank loops which favor in the disordered phase. The higher stacking fault energy in the ordered phase renders it difficult to form stacking fault tetrahedra

1. Introduction

Advanced nuclear reactors with concomitant stringent technological requirement have boosted the demand for new materials able to operate in extreme conditions. The search for materials with specific mechanical properties, superior radiation tolerance, and good corrosion resistance has led to increasing research of multi-principal element alloys (MPEAs) [1–3], including high-entropy alloys (HEAs). In contrast to conventional alloys, MPEAs are random solid solutions based on simple crystal structure with two or more multiple principal elements (five or more are referred to as HEAs) [4]. Randomly occupying of multiple elemental species in the lattice site of these alloys results in local disordered chemical environments and unique site-to-site lattice distortions [5], thereby providing possibilities to obtain exceptional properties, especially the radiation tolerance. The extreme chemical disorder can remarkably modify defect kinetics and heat dissipation, leading to low damage accumulation and self-recovery [6,7].

However, total chemical disorder is virtually uncommon in MPEAs. Miracle studied 408 MPEAs with 648 unique microstructures [8], where 48% the total reported microstructures are single-phase solid solution, 52% have intermetallic phase or have only intermetallic phase. The results suggest that the intermetallic phases widely exist inside MPEAs. These phases are usually based on locally ordered structures, which have a pronounced effect on radiation effects. First-principal study demonstrated that the formation and migration energy of point defects in concentrated binary and ternary alloys can be strongly affected by the configuration of nearest neighboring atoms [9]. Molecular dynamics (MD) simulations found that defect diffusion is slow-down in the ordered Ni–Fe alloy compared with its disordered counterparts, indicating that defect evolution may be significantly delayed by embedding ordered structures into bulk disordered alloys [10]. It can be inferred that the ordered structures wouldn't impair the radiation tolerance of MPEAs. Instead, such structures can be deliberately introduced into MPEAs to optimize their performance. Numerous relevant studies focus on mechanical properties and obtained exceptional improvement [11–13]. However, the effects of ordered structure on radiation tolerance are rarely reported. A comprehensive comparison of radiation response between the ordered and disordered phases is the basis for the candidate materials of advanced nuclear system extending to multi-phase solid solution alloys.

In this work, the irradiation-induced defect production and evolution were investigated from MD perspectives. The equiatomic NiFe was selected as the object because its disordered state possesses good radiation tolerance [14], and the same atomic ratio ordered phase is a

* Corresponding author.
E-mail address: tangxiaobin@nuaa.edu.cn (X. Tang).

https://doi.org/10.1016/j.nimb.2021.04.012
Received 18 December 2020; Received in revised form 14 April 2021; Accepted 20 April 2021
Available online 3 May 2021

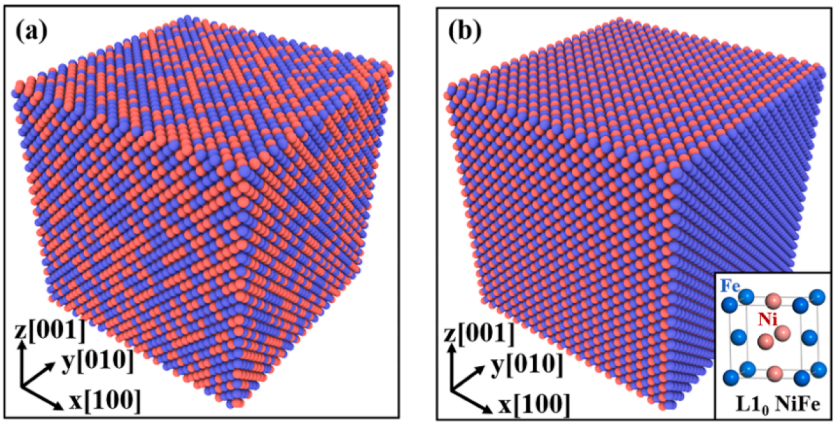

Fig. 1. Simulation models of (a) disordered NiFe and (b) ordered NiFe, the inset is the unit cell of $L1_0$ NiFe.

ground state in the Ni–Fe phase diagram, that is, $L1_0$ NiFe [15]. This study aimed to explore the effects of order and disorder with respect to the behavior and laws of interstitial, vacancy, and their corresponding typical clusters.

2. Methods

All atomic simulations in this study were conducted with the MD code LAMMPS [16]. More specifically, collision cascade simulations at varying energies were performed to provide a general understanding of the primary damage production in terms of residual point defects. Defect insertion methods were adopted to explore the dynamics of interstitial and dislocation loops, and dislocation-enhanced cascade simulations were conducted to learn the stacking fault tetrahedra (SFT) formation. The detailed reasons for choosing these approaches will be explained in the Result and discussion section, and this section only describes the modeling process and parameter settings. The simulation models of $L1_0$ NiFe and its disordered counterpart are displayed in Fig. 1. In the disordered phase, Ni and Fe atoms are randomly placed to replicate the random nature of solid solutions. For the ordered phase, the model is the supercell of the $L1_0$ structure shown in the inset of Fig. 1(b). The embedded atom method potential developed by Béland et al. [17] was used to describe the interactions between the Ni and Fe atoms. In spite of the commonly used potential, 2011 Bonny FeNiCr potential [18], has been verified to give defect energetics and defect dynamics in extremely good agreement with ab initio calculations. Béland potential is the reparametrization of the short-range forces based on Bonny potential for the sake of providing more accurate prediction of primary damage production.

In cascade simulations, the simulation box is as large as $142 \times 142 \times 142$ Å^3 (containing 256,000 atoms, lattice constant $a_0 = 3.55$ Å) or $178 \times 178 \times 178$ Å^3 (containing 500,000 atoms) depending on the PKA energy (5,10 keV or 20 keV). The atoms found within a 0.5 nm-thick layer at all sides of the box were forced to maintain a constant temperature (300 K) through Nose–Hoover heat bath [19]. Thus, the excess kinetic energy introduced by the PKA can be dissipated as that in experimental situations. A variable time-step was used to accurately capture the atomic forces and limit the distance traveled by atoms between timesteps. Each simulation lasted from 30 ps to 50 ps until no energetic interactions remained in the system. Forty independent cascade simulations were conducted for each model to reduce the statistical errors.

For the defect insertion method, a small ($71 \times 71 \times 71$ Å^3, containing 32,000 atoms) box was used for computation efficiency. Interstitial atoms (0.5 at. %) were randomly introduced into the boxes, and the simulations were performed for 250 ns at 300 K and 0 pressure. This simulation time is sufficient to allow all the possible interaction events in the primary stage to occur. An edge dislocation was created via the "strain and spline" approach [20] in dislocation-enhanced cascade simulations. Forty independent cascade simulations were performed at 20 keV PKA energy.

MD visualizations were rendered with the open tool OVITO [21]. Defects were characterized through Wigner–Seitz (W–S) defect analysis [22] and common neighbor analysis (CNA) [23]. The former was applied to analyze the type and number of point defects, and the latter was used to display the irregular atoms. Dislocation extraction algorithm (DXA) [24] was utilized to analyze the type and volume of dislocation. The dislocation was distinguished by different colored lines and volumes. The cluster size distribution was analyzed via calculating the distance between each defect and all other defects. Defects within a fixed cut-off radius from each other were interpreted as a part of the same defect cluster. All the analyzing approaches were implanted into the OVITO.

3. Result and discussion

3.1. Residual Frenkel pair (FP)

The collision cascades in ordered and disordered NiFe were performed with the PKA energy of 5, 10, and 20 keV. The evolution of damage production in terms of FP was analyzed. Three energy cascades exhibited the similar trends of FP time evolution. Thus, the result of the simulations of the 10 keV cascades was taken as a typical instance. A logarithmic time-profile of the FP number and linear time-profile of temperature are shown in Fig. 2. The final FP number of three PKA energies cascades is shown in Table 1. All the presented results are the averages of 40 individual simulation runs. Cascades process can be broken down primarily into two stages, namely, ballistic and kinetic stages. The ballistic stage can be further split into supersonic phase and sonic phase in accordance with the change of slope [25]. The first phase creates permanent defects along the trajectory of supersonic shockwave. The second phase merely causes the elastic displacements without creating new permanent defects. The final stage recovers from the ballistic stage and has a rapid decrease in defects [26].

The ordered and disordered NiFe have approximately coincident profiles in the supersonic phase, indicating that the ordered configuration has minimal influence on the permanent defect created by supersonic shockwave. The difference between ordered and disordered NiFe appears at the sonic phase. The high intrinsic interatomic stress makes the disordered configuration easy to transform to amorphous during collision cascade [27], resulting in a high peak value of FP in sonic stage, while it has nothing to do with the final number of defects, as previously explained. It is worth noting the huge standard errors in the sonic phase, which imply a great difference of FP number emerged in the different simulation runs (peak value from 400 to 1400). The FP number in the sonic phase crucially relates to the trajectory of shockwave presented in

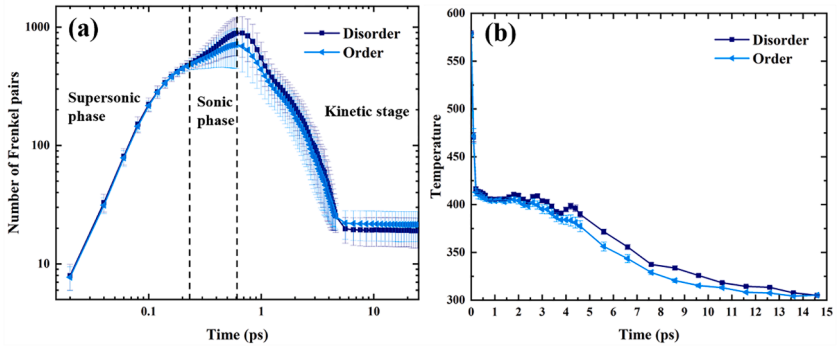

Fig. 2. (a) Logarithmic time-profile of the FP number during the cascade simulation with the PKA energy of 10 keV. The three stages of the cascade are divided by the dash line. (b) Time-profile of temperature during the cascade.

Table 1
Residual FP number of three PKA energies cascades.

PKA energies (keV)	Disordered NiFe	Ordered NiFe
5	10.7 ± 1.7	13.3 ± 1.8
10	19.0 ± 2.7	21.5 ± 3.1
20	44.0 ± 6.0	44.5 ± 5.6

Table 2
Percentages of 40 cases of single effect cascades at 20 keV that form three different types of cluster.

Defect cluster types	Disordered NiFe	Ordered NiFe
Shockley partial loops	20%	25%
Frank dislocation loops	17.5%	20%
SFT	17.5%	7.5%

different runs by inspecting the damage zone evolution. The short trajectory means more concentrated damaged zone and makes the temperature to remain higher, resulting in more atoms melt into liquid-like stage and counted as defect. The long trajectory is the opposite. However, we did not find the proportional relationship between the peak and final values of FP. It also reinforces the principle that the sonic phase creating no new permanent defects.

To date, the effects of ballistic stage, including supersonic and sonic phases, on the final FP numbers have no difference between the ordered and disordered NiFe. It can be inferred that the quantity difference presented in Table 1 is obtained from the kinetic stage. As shown in Fig. 2(b), the temperature evolutions of two materials rapidly decrease roughly in the supersonic phase and then transform to a moderate decline in the following stage. The temperature of disordered NiFe remains higher than the ordered one. The elevated temperature in disordered NiFe enhances the defect diffusion, leading to an accelerated recombination. Therefore, the number of residual point defects in disordered NiFe with three PKA energies are all lower than the ordered. High temperatures at the center of the cascade cores remain different times in different materials depending on thermal conductivities. It is commonly recognized that disorder reduces electron and phonon conductivity. In the short time-scales related to thermal spikes induced by collision cascades, phonons become the relevant energy carrier [28]. Thus, the lattice thermal conductivities of two materials were calculated adopting the Green-Kubo methodology. At 300 K, the measurement for ordered and disordered NiFe is 30.4 and 8.3 W $(mK)^{-1}$, respectively. The results valid that disordered NiFe with lower thermal conductivity is beneficial to the recombination of FPs.

It is noteworthy that the difference in the final FP number between two materials is reduced with the increase in the PKA energies. This phenomenon is consistent with the result in previous study that the damage production is only related to thermal conductivity at energies of 20 keV and less [29]. The disordered alloys do not enhance FP recombination by low thermal conductivity because direct cluster formation occurs in 20 keV collision cascade. Other mechanisms are responsible for the defect evolution and cluster formation in collision cascades with the PKA energy of 20 keV, which will be investigated in the next sections.

3.2. Interstitial dislocation loop

Different from the low energy (5, 10 keV) collision cascades only producing individual point defects, defect clusters, such as interstitial type dislocation loop and SFT, are formed at 20 keV. Some differences are found between the ordered and disordered NiFe. Combining the result of interstitial insertion and dislocation-enhanced cascade, more sluggish formation behavior of typical clusters is found in the ordered phase, which is beneficial to the radiation tolerance. The percentages of 40 cases of single effect cascades at 20 keV that form three different types of cluster (Shockley partial loops, Frank dislocation loop and SFT) are presented in Table 2. This section focuses on the dislocation structure, and SFT will be discussed in the next section. The message obtained from the data is that dislocation forms more frequently in the ordered phase than the disordered phase, and the occurrences of Shockley partial loops are more frequent than Frank dislocation loops in the two materials.

It is commonly recognized that these two loops are formed by the agglomeration of interstitials. Hence, a defect insertion method only focuses on interstitial evolution was applied. An important feature of this method is that one can control the defect type [30]. Several studies replicated the experimentally observed results by adopting this approach [31–33]. The final snapshots of the simulation box containing 0.5 at. % interstitial after 250 ns relaxation identified by W–S (Fig. 3(a), (b)) and DXA (Fig. 3(c), (d)) are presented in Fig. 3. The number of interstitials in different cluster size distributions via cluster analysis is included (Fig. 3(e)). Both the snapshots and histogram show that the interstitial cluster in disordered NiFe has bigger size with lower density. The explanation can be the slower defect diffusion in the ordered NiFe phases than the disordered phase because of the decrease in effective coordination number for nearest-neighbor defect jumps [10]. The ordered arrangement of elements limiting the mobility of interstitials to delay their accumulation and long-distance travel, leading to the formation of small and dispersed cluster. This mechanism is also responsible for the result of the cascade simulation that the interstitial loop forms more in the ordered phase than the disordered phase. The type of dislocation structure is found to vary in different materials. The number of Shockley partial loops formed in the disordered phase is slightly higher than Frank loops, which is consistent with the results of cascade simulation. By contrast, only one Frank loop is formed in the ordered phase.

The contradiction of the evolution of dislocation structures highlights the necessity of good understanding of the migration behavior of interstitial in the studied materials. A single Fe atom is introduced at the

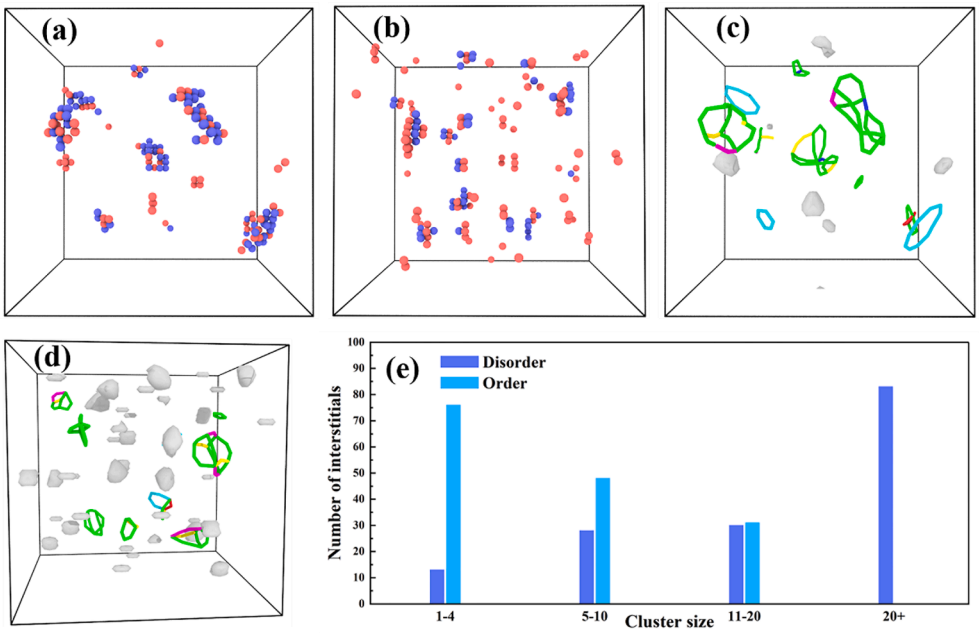

Fig. 3. Interstitial evolution after 250 ns relaxation. W–S defect analysis results of (a) disordered NiFe and (b) ordered NiFe. DXA results of (c) disordered and (d) ordered. The lines of different colors represent the dislocations with different Burgers vectors, where green is a Shockley, pink is a stair-rod, light blue is a Frank, yellow is a Hirth, dark blue is a perfect dislocation, and red is other. The white volumes represent the defect clusters. (e) Number of interstitials in different cluster size distributions of two materials. (For interpretation of the references to colour in this figure legend, the reader is referred to the web version of this article.)

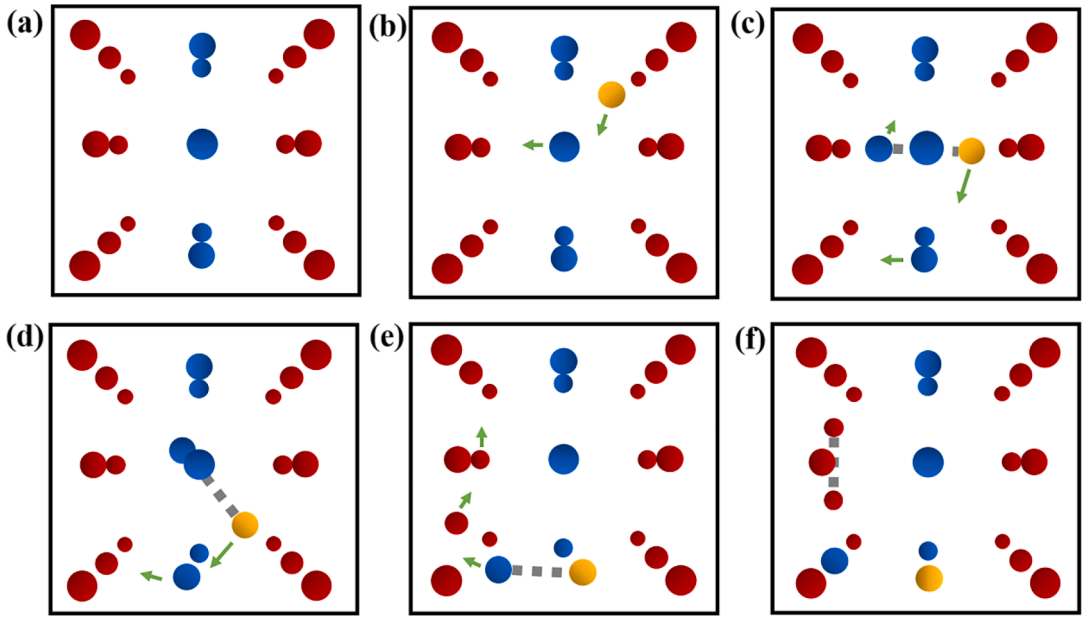

Fig. 4. Schematic views of the migration pathway for the interstitial introduced in the ordered configuration. The red, blue, and yellow spheres represent the Ni, Fe atoms and deliberately introduce the interstitial. The movement directions at the next moment are marked by green arrow. The dash line suggests the dumbbell formed by two atoms. (For interpretation of the references to colour in this figure legend, the reader is referred to the web version of this article.)

interstitial site in the Fe layer of the ordered box, and its migration pathway is shown in Fig. 4. The diffusion of an interstitial preferably follows a shifting and rotation mechanism [34] that a dumbbell interstitial shifts to its nearest neighbor, followed by a rotation to another dumbbell. The interstitial is stable in the Ni layer in the form of Ni–Ni dumbbell. With additional simulations, whether Ni or Fe interstitial is introduced in the Ni or Fe layer, they all finally form a Ni–Ni dumbbell in the Ni layer. This condition is in accordance with the formation energies calculation of interstitial dumbbells in ordered NiFe alloys [10], where the Ni–Ni dumbbell in the Ni layer has the lowest formation energy and makes the formation favorable. The mechanism affects the types of dislocation as present in Fig. 3 in the following way: first, the formation of close-packed {1 1 1} planar loop is a characteristic nature in face-centered cubic (fcc) materials [30]. Thus, Frank dislocation loop is formed in the two studied materials. Second, the preferential diffusion mechanism restricts interlayer diffusion in the ordered phase, where the Ni and Fe layers are alternately arranged along the [1 0 0] direction (Fig. 1). This condition not only results in slower interstitial migration and aggregation processes, but also inhibits the interstitials to migrate to {1 1 1} planar to form Frank loops. With the effects of two competitive factors, only one Frank loop is formed in the ordered phase, and the rest are Shockley partial chains.

However, the result of the ordered phase by cascade simulation do not follow the same behavior with the defect insertion simulation. The proportion of Frank loops is significantly high in the cascade simulation. The divergence occurs from the ballistic stage, which is not captured in

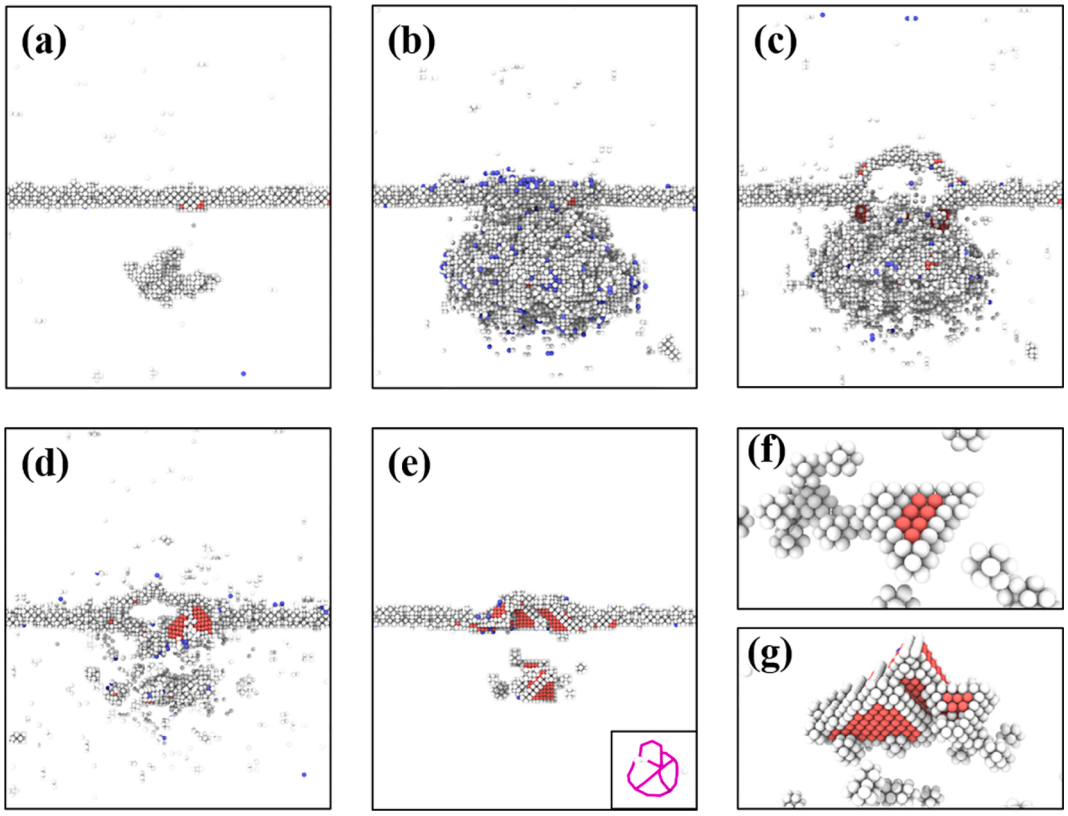

Fig. 5. (a)–(e) Snapshots of the cascade process induced by the PKA placed 45 Å below the edge dislocation. Inset in (e) is the result of DXA of the cluster under dislocation, and the pink lines represent stair-rod. Typical morphologies of SFT formed in (f) single crystal and (g) pre-existing dislocation box. Visualizations are rendered with CNA. (For interpretation of the references to colour in this figure legend, the reader is referred to the web version of this article.)

defect insertion simulation. This stage causes a sharp rise in temperature with the expansion of thermal spike during collision cascade as shown in Fig. 2(b). In this case, the interstitial in ordered phase breaks free from the bondage of the Ni layer, and the {1 1 1} migration becomes dominant. Therefore, the ordered phase forms a number of Frank type dislocation loops similar to the disordered phase. It stresses a further consideration about the influence of temperature when applying defect insertion method.

3.3. SFT

The growth of dislocation loops formed by the agglomeration of interstitials is significantly inhibited in the ordered NiFe. Moreover, the data obtained by 20 keV PKA cascades (Table 2) shows that the occurrences of SFT formed by the agglomeration of vacancies are reduced in the ordered phase. Nevertheless, these data imply that the formation of SFT by direct collision cascade is a low probability event. It is insufficient for the comparative study of two materials because of its occasionality. A method that can promote the vacancy production and induce large defect clustering needs to be employed. The defect insertion method can achieve this goal easily [30]. Whereas, the ballistic stage bypassed in this method may result in an inaccurate prediction of clustering behavior as explained above, especially for the case that the migration of vacancy is sensitive to temperature. Considering the intrinsic dislocations in the MD simulations of collision cascades might provide reliable explanations [35], because dislocations universally exist in most metals. The pre-existing dislocation will exhibit an evident absorption preference for the interstitials at the case of once cascade simulation. That may leave behind quiet more vacancies in the core of collision cascade than the simulation in the perfect single crystal and facilitate the nucleation of the vacancy clusters.

Fig. 5 shows the temporal evolution of defects in the cascade simulation with pre-existing edge dislocation. A PKA with 20 keV was introduced at a certain distance (d = 45 Å) from the dislocation and directly toward it. Varying distances have been performed, and 45 Å is the best distance that enables the cascade zone to “hang” on the dislocation line, as shown in Fig. 5(b) [35]. In this case, the maximum number of vacancies are left to form a cluster. The defect temporal evolution with dislocation also follows the typical melting and recrystallization process. The dislocation line partially climbs upward by the shockwave (Fig. 5(c)). At the end of the recrystallization, the upward part is filled with atoms again (Fig. 5(e)), which validating the absorption effect of dislocations on interstitial atoms. In the meanwhile, the vacancies in the cascade core with few interstitials recombine and agglomerate into a large cluster. It turns out to be a SFT by DXA for it is bounded by stair-rod partial dislocations (Fig. 5(e) inset).

By inspecting the morphologies of SFT in each cascade simulation, we find that different with the perfectly shaped SFTs formed in perfect single crystal (Fig. 5(f)), most SFTs formed in the pre-existing dislocation box are overlapping (two SFTs stuck to each other, Fig. 5(g)). Such phenomenon is commonly observed in the transmission electron microscopy examinations of irradiated fcc metals [36]. In this work, the difference in these morphologies is attributed to the varying number of vacancies in the clusters directly generated by the cascade collision. It can be easily understood that high vacancy concentration leads to the formation of overlapping SFTs in dislocation-enhanced simulation, which also showing the reliability of applying this model to study SFT.

The difference between the two studied materials is explored. 20% of the cascade in the ordered phase forms SFT, and the disordered one is 50%. It retains the similar trend with the results in perfect single crystal (Table 2) that the SFT forms more usually in the disordered phase than in the ordered phase. Moreover, the probabilities are significantly increased in the dislocation-enhanced cascade simulation, validating that the ordered phase is difficult to form SFT. The formation of SFTs has

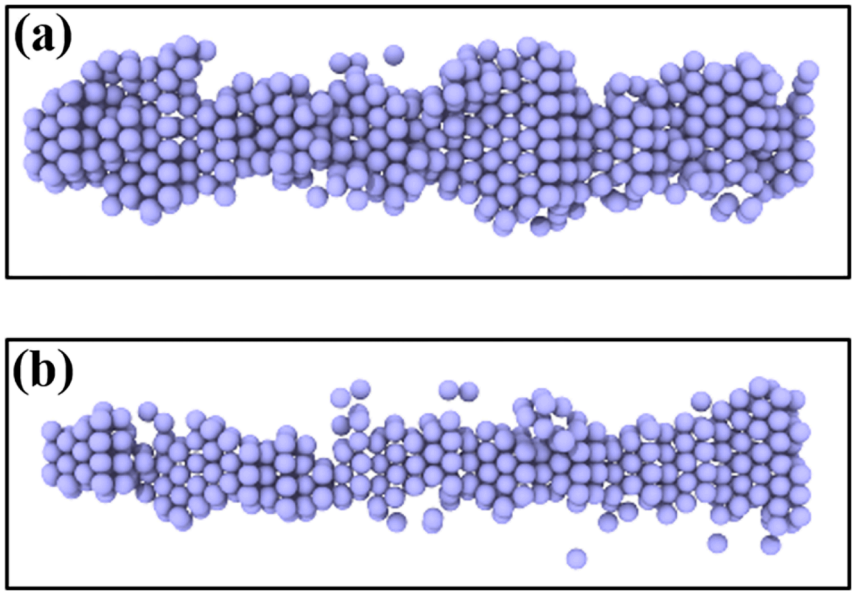

Fig. 6. Snapshots of edge dislocations in (a) disordered and (b) ordered NiFe. The visible atoms form the stacking fault generated by the separation of the dislocation into two partials.

a strong correlation with the stacking fault energy (SFE) of materials. Thus, the SFEs of two materials were qualitatively investigated through the splitting reaction of perfect dislocation. The perfect dislocation with Burgers vector $b = 1/2[1\,1\,0]$ spontaneously splits up into two Shockley partials with Burgers vector $b = 1/6[1\,1\,2]$ in accordance with the reaction [37]:$b_1{:}\frac{1}{2}\langle 110\rangle \rightarrow b_2{:}\frac{1}{6}\langle 211\rangle + b_3{:}\frac{1}{6}\langle 12\bar{1}\rangle$

$$(1)\text{Perfect}\left(b = \tfrac{1}{2}\langle 110\rangle{:}\ b^2 = \tfrac{a_0^2}{4}\left(1^2+1^2+0^2\right) = \tfrac{a_0^2}{2}\right)$$

$$(2)\text{Shockley}\left(b = \tfrac{1}{6}\langle 112\rangle{:}\ b^2 = \tfrac{a_0^2}{36}\left(1^2+1^2+2^2\right) = \tfrac{a_0^2}{6}\right) \quad (3)$$

The energy of a dislocation is proportional to the square of the magnitude of its Burgers vector. Equations (2) and (3) suggest that the splitting reaction is energetically favorable because $b_1^2 = a_0^2/2$ corresponding to the perfect dislocation is greater than $b_2^2 + b_3^2 = a_0^2/3$ corresponding to the two Shockley partials. The SFE (γ) is inversely proportional to the distance (d) between the two partials, which can be estimated as $\gamma = \frac{Gb^2}{4\pi d}$ (4)

where G is the shear modulus, and b is the length of the Burgers vector. The snapshots of the edge dislocations in the two materials at 300 K are shown in Fig. 6. Assuming that the shear modulus does not change, we can deduce that ordered phase shows higher SFE than the disordered phase, which is consistent with the calculation results (59 mJ/m^2 for ordered NiFe and 32 mJ/m^2 for disordered NiFe) in Zhao's work [38]. And the results accord with the fact that SFTs are usually formed in materials with a low SFE [37].

4. Conclusion

Cascade simulation at varying PKA energy, defect insertion method, and dislocation-enhanced cascade simulations were conducted to investigate the residual FP, interstitial dislocation loop, and SFT, respectively. Three key factors dominate the difference in the evolution of three types of defects between the ordered and disordered NiFe. The conclusions are as follows:

1) The intrinsic chemical disorder reduces the thermal conductivity in the disordered phase, which is beneficial for FP recombination during the kinetic stage in collision cascade. With the increase in PKA energy, the effect of thermal conductivity is weakened by direct cluster formation.
2) The ordered arrangement of elements limiting the mobility of interstitials to delay their accumulation, leading to the formation of interstitial clusters with smaller size and higher density. This condition also responsible for the irregular type of dislocation loops, which is reflected in the fact that the ordered phase tends to form Shockley partial loops rather than Frank loops favor in the disordered phase. This difference will disappear under the annealing effect of the thermal peak in cascade collision.
3) The different distances between two Shockley partials arising from the splitting reaction of perfect dislocation indicate the higher SFE in the ordered phase than in the disordered phase, rendering the ordered phase difficult to form SFT.

These results present a sluggish evolution of the overall microstructure in the ordered phase under radiation. Embedding such structures into bulk disordered alloys may elevate the radiation tolerance.

CRediT authorship contribution statement

Guojia Ge: Conceptualization, Methodology, Software, Validation, Formal analysis, Investigation, Data Curation, Writing - original draft, Writing - review & editing. **Feida Chen**: Conceptualization, Writing - original draft, Funding acquisition. **Xiaobin Tang**: Writing - original draft, Supervision, Project administration, Funding acquisition. **Changyuan Li:** Methodology, Writing - review & editing. **Jing Gao**: Writing - original draft, **Songyuan Li**: Investigation. **Zhenlong Geng**: Investigation.

Declaration of Competing Interest

The authors declare that they have no known competing financial interests or personal relationships that could have appeared to influence the work reported in this paper.

Acknowledgements

This work is supported from the National Natural Science Foundation of China (Grant No. 11705087), the Natural Science Foundation of Jiangsu Province (Grant No. BK20170776) and the Postgraduate Research & Practice Innovation Program of Jiangsu Province (Grant No. KYCX20_0196).

References

[1] B. Gludovatz, A. Hohenwarter, D. Catoor, E.H. Chang, E.P. George, R.O. Ritchie, A fracture-resistant high-entropy alloy for cryogenic applications, Science 345 (6201) (2014) 1153–1158, https://doi.org/10.1126/science:1254581.

[2] C. Lu, L. Niu, N. Chen, K.e. Jin, T. Yang, P. Xiu, Y. Zhang, F. Gao, H. Bei, S. Shi, M.-R. He, I.M. Robertson, W.J. Weber, L. Wang, Enhancing radiation tolerance by controlling defect mobility and migration pathways in multicomponent single-phase alloys, Nat. Commun. 7 (1) (2016), https://doi.org/10.1038/ncomms13564.

[3] Y.L. Chou, J.W. Yeh, H.C. Shih, The effect of molybdenum on the corrosion behaviour of the high-entropy alloys Co1.5CrFeNi1.5Ti0.5Mox in aqueous environments, Corros. Sci. 52 (8) (2010) 2571–2581, https://doi.org/10.1016/j.corsci.2010.04.004.

[4] J.-W. Yeh, S.-K. Chen, S.-J. Lin, J.-Y. Gan, T.-S. Chin, T.-T. Shun, C.-H. Tsau, S.-Y. Chang, Nanostructured high-entropy alloys with multiple principal elements: Novel alloy design concepts and outcomes, Adv. Eng. Mater. 6 (5) (2004) 299–303.

[5] Y. Zhang, G.M. Stocks, K.e. Jin, C. Lu, H. Bei, B.C. Sales, L. Wang, L.K. Béland, R. E. Stoller, G.D. Samolyuk, M. Caro, A. Caro, W.J. Weber, Influence of chemical disorder on energy dissipation and defect evolution in concentrated solid solution alloys, Nat. Commun. 6 (1) (2015), https://doi.org/10.1038/ncomms9736.

[6] K. Jin, H. Bei, Single-phase concentrated solid-solution alloys: Bridging intrinsic transport properties and irradiation resistance, Front Mater. 5 (2018) 1–11, https://doi.org/10.3389/fmats.2018.00026.

[7] T. Yang, C. Li, S.J. Zinkle, S. Zhao, H. Bei, Y. Zhang, Irradiation responses and defect behavior of single-phase concentrated solid solution alloys, J. Mater. Res. 33 (19) (2018) 3077–3091, https://doi.org/10.1557/jmr.2018.285.

[8] D.B. Miracle, O.N. Senkov, A critical review of high entropy alloys and related concepts, Acta Mater. 122 (2017) 448–511, https://doi.org/10.1016/j.actamat.2016.08.081.

[9] J.B. Piochaud, T.P.C. Klaver, G. Adjanor, P. Olsson, C. Domain, C.S. Becquart, First-principles study of point defects in an fcc Fe-10Ni-20Cr model alloy, Phys. Rev. B: Condens. Matter Mater. Phys. 89 (2) (2014), https://doi.org/10.1103/PhysRevB.89.024101.

[10] S. Zhao, Y. Osetsky, Y. Zhang, Diffusion of point defects in ordered and disordered Ni–Fe alloys, J. Alloys Compd. 805 (2019) 1175–1183, https://doi.org/10.1016/j.jallcom.2019.07.142.

[11] T. Yang, Y.L. Zhao, Y. Tong, Z.B. Jiao, J. Wei, J.X. Cai, X.D. Han, D. Chen, A. Hu, J. J. Kai, K. Lu, Y. Liu, C.T. Liu, Multicomponent intermetallic nanoparticles and superb mechanical behaviors of complex alloys, Science 362 (6417) (2018) 933–937, https://doi.org/10.1126/science:aas8815.

[12] L.u. Zhang, Y. Zhou, X.i. Jin, X. Du, B. Li, Precipitation-hardened high entropy alloys with excellent tensile properties, Mater. Sci. Eng. A 732 (2018) 186–191, https://doi.org/10.1016/j.msea.2018.06.102.

[13] N.D. Stepanov, N.Y. Yurchenko, V.S. Sokolovsky, M.A. Tikhonovsky, G. A. Salishchev, An AlNbTiVZr0.5 high-entropy alloy combining high specific strength and good ductility, Mater. Lett. 161 (2015) 136–139, https://doi.org/10.1016/j.matlet.2015.08.099.

[14] C. Lu, T. Yang, L. Niu, Q. Peng, K.e. Jin, M.L. Crespillo, G. Velisa, H. Xue, F. Zhang, P. Xiu, Y. Zhang, F. Gao, H. Bei, W.J. Weber, L. Wang, Interstitial migration behavior and defect evolution in ion irradiated pure nickel and Ni-xFe binary alloys, J. Nucl. Mater. 509 (2018) 237–244, https://doi.org/10.1016/j.jnucmat.2018.07.006.

[15] S.V. Barabash, R.V. Chepulskii, V. Blum, A. Zunger, First-principles determination of low-temperature order and ground states of Fe-Ni, Fe-Pd, and Fe-Pt, Phys. Rev. B: Condens. Matter Mater. Phys. 80 (2009) 1–4, https://doi.org/10.1103/PhysRevB.80.220201.

[16] S. Plimpton, Fast parallel algorithms for short-range molecular dynamics, J. Comput. Phys. 117 (1995) 1–19.

[17] L.K. Béland, A. Tamm, S. Mu, G. Samolyuk, Y. Osetsky, A. Aabloo, M. Klintenberg, A. Caro, R. Stoller, Accurate classical short-range forces for the study of collision cascades in Fe–Ni–Cr, Comput. Phys. Commun. 219 (2017) 11–19, https://doi.org/10.1016/j.cpc.2017.05.001.

[18] G. Bonny, D. Terentyev, R.C. Pasianot, S. Poncé, A. Bakaev, Interatomic potential to study plasticity in stainless steels: The FeNiCr model alloy, Model Simul. Mater. Sci. Eng. 19 (8) (2011) 085008, https://doi.org/10.1088/0965-0393/19/8/085008.

[19] G.J. Martyna, M.L. Klein, M. Tuckerman, Nosé-Hoover chains: The canonical ensemble via continuous dynamics, J. Chem. Phys. 97 (4) (1992) 2635–2643, https://doi.org/10.1063/1.463940.

[20] V.S. Krasnikov, A.E. Mayer, Y.N. Osetsky, D.J. Bacon, An Atomic-level model for studying the dynamics of edge dislocations in metals influence of local stresses on motion of edge dislocation in aluminum, Model Simul. Mater. Sci. Eng. 11 (2003) 427–446.

[21] A. Stukowski, Visualization and analysis of atomistic simulation data with OVITO-the Open Visualization Tool, Model Simul. Mater. Sci. Eng. 18 (1) (2010) 015012, https://doi.org/10.1088/0965-0393/18/1/015012.

[22] K. Nordlund, M. Ghaly, R.S. Averback, M. Caturla, T. Diaz de la Rubia, J. Tarus, Defect production in collision cascades in elemental semiconductors and fcc metals, Phys. Rev. B: Condens. Matter Mater. Phys. 57 (13) (1998) 7556–7570, https://doi.org/10.1103/PhysRevB.57.7556.

[23] J.D. Honeycutt, H.C. Andersen, Molecular dynamics study of melting and freezing of small Lennard-Jones clusters, J. Phys. Chem. 91 (19) (1987) 4950–4963, https://doi.org/10.1021/j100303a014.

[24] A. Stukowski, V.V. Bulatov, A. Arsenlis, Automated identification and indexing of dislocations in crystal interfaces, Model. Simul. Mater. Sci. Eng. 20 (8) (2012) 085007, https://doi.org/10.1088/0965-0393/20/8/085007.

[25] A.F. Calder, D.J. Bacon, A.V. Barashev, Y.N. Osetsky, On the origin of large interstitial clusters in displacement cascades, Philos. Mag. 90 (7-8) (2010) 863–884, https://doi.org/10.1080/14786430903117141.

[26] L.K. Béland, Y.N. Osetsky, R.E. Stoller, The effect of alloying nickel with iron on the supersonic ballistic stage of high energy displacement cascades, Acta Mater. 116 (2016) 136–142, https://doi.org/10.1016/j.actamat.2016.06.031.

[27] T. Nagase, P.D. Rack, J.H. Noh, T. Egami, In-situ TEM observation of structural changes in nano-crystalline CoCrCuFeNi multicomponent high-entropy alloy (HEA) under fast electron irradiation by high voltage electron microscopy (HVEM), Intermetallics 59 (2015) 32–42, https://doi.org/10.1016/j.intermet.2014.12.007.

[28] M. Caro, L.K. Béland, G.D. Samolyuk, R.E. Stoller, A. Caro, Lattice thermal conductivity of multi-component alloys, J. Alloys Compd. 648 (2015) 408–413, https://doi.org/10.1016/j.jallcom.2015.06.035.

[29] L.K. Béland, C. Lu, Y.N. Osetskiy, G.D. Samolyuk, A. Caro, L. Wang, R.E. Stoller, Features of primary damage by high energy displacement cascades in concentrated Ni-based alloys, J. Appl. Phys. 119 (8) (2016) 085901, https://doi.org/10.1063/1.4942533.

[30] D.S. Aidhy, C. Lu, K.e. Jin, H. Bei, Y. Zhang, L. Wang, W.J. Weber, Point defect evolution in Ni, NiFe and NiCr alloys from atomistic simulations and irradiation experiments, Acta Mater. 99 (2015) 69–76, https://doi.org/10.1016/j.actamat.2015.08.007.

[31] Y. Zhang, D.S. Aidhy, T. Varga, S. Moll, P.D. Edmondson, F. Namavar, K.e. Jin, C. N. Ostrouchov, W.J. Weber, The effect of electronic energy loss on irradiation-induced grain growth in nanocrystalline oxides, Phys. Chem. Chem. Phys. 16 (17) (2014) 8051–8059, https://doi.org/10.1039/C4CP00392F.

[32] D.S. Aidhy, Y. Zhang, W.J. Weber, Radiation damage in cubic ZrO2 and yttria-stabilized zirconia from molecular dynamics simulations, Scr. Mater. 98 (2015) 16–19, https://doi.org/10.1016/j.scriptamat.2014.10.036.

[33] A.H. Quadery, S. Pacheco, A. Au, N. Rizzacasa, J. Nichols, T. Le, C. Glasscock, P. K. Schelling, Atomic-scale simulation of space weathering in olivine and orthopyroxene, J. Geophys. Res. Planets 120 (4) (2015) 643–661, https://doi.org/10.1002/2014JE004683.

[34] S. Zhao, G.M. Stocks, Y. Zhang, Defect energetics of concentrated solid-solution alloys from ab initio calculations: Ni0.5Co0.5, Ni0.5Fe0.5, Ni0.8Fe0.2 and Ni0.8Cr0.2, Phys. Chem. Chem. Phys. 18 (34) (2016) 24043–24056, https://doi.org/10.1039/C6CP05161H.

[35] W. Zhou, J. Tian, J. Zheng, J. Xue, S. Peng, Dislocation-enhanced experimental-scale vacancy loop formation in hcp zirconium in one single collision cascade, Sci. Rep. 6 (1) (2016), https://doi.org/10.1038/srep21034.

[36] R. Schäublin *, Z. Yao, N. Baluc, M. Victoria, Irradiation-induced stacking fault tetrahedra in fcc metals, Philos. Mag. 85 (4-7) (2005) 769–777, https://doi.org/10.1080/14786430412331319929.

[37] D. Hull, D.J. Bacon, Introduction to dislocations, vol. 37, Elsevier, 2011.

[38] S. Zhao, D.a. Chen, G. Yeli, J.J. Kai, Atomistic insight into the effects of order, disorder and their interface on defect evolution, J Alloys Compd. 859 (2021) 157770, https://doi.org/10.1016/j.jallcom.2020.157770.